

Manifestations of Classical Chaos in the Energy Level Spectrum of a Quantum Well

T. M. Fromhold, P. B. Wilkinson, F. W. Sheard, L. Eaves, J. Miao, and G. Edwards
Department of Physics, University of Nottingham, Nottingham NG7 2RD, United Kingdom
 (Received 9 August 1994)

The electronic energy levels and eigenfunctions of a wide potential well in a double barrier structure with a large tilted magnetic field are investigated in the regime of strong classical chaos. Periodic modulations of the level density are identified and related to distinct unstable closed classical orbits. Single periodic orbits “scar” the wave functions corresponding to regular subsets of energy levels determined by quantizing the classical action. Pronounced features in the tunneling rates into the well provide an experimentally accessible means of studying wave-function scarring.

PACS numbers: 73.20.Dx, 05.45.+b, 73.40.Gk, 73.40.Kp

The correspondence between a chaotic classical system and its quantum analog is of fundamental interest. Theoretical studies have highlighted the importance of unstable periodic classical orbits which produce regular clustering of the quantized energy levels [1,2] and “scar” the associated wave functions [3]. The influence of classical chaos on two-dimensional quantum transport has been studied using antidot superlattices [4] and billiard stadia [5]. The link between the classical and quantum pictures of chaotic electron dynamics has also been explored in recent experiments on GaAs/(AlGa)As resonant tunneling diodes (RTD's) containing a wide (120 nm) potential well [6]. In the presence of a large tilted magnetic field, the classical orbits are chaotic. However, unstable closed orbits exist and control the resonant tunneling peaks in the current-voltage characteristics of the RTD's.

In this Letter, we calculate the quantized energy levels and eigenfunctions of the wide GaAs quantum well (QW) in a RTD, when a strong magnetic field B is applied at an angle θ normal to the barriers. For values of θ where the system exhibits strong classical chaos, we identify periodic modulations in the density of levels which we associate with distinct types of unstable periodic orbit. The distribution of nearest-neighbor level spacings is shown to obey Wigner statistics. The wave functions corresponding to distinct subsets of energy levels embedded within the full spectrum exhibit scarring by a particular closed orbit. For each scarred wave function, the number of antinodes along the corresponding orbital path defines a quantum number which we relate to the classical action of the orbit.

The potential energy of an electron in the RTD is shown schematically in Fig. 1. Electrons are injected into the QW from a two-dimensional electron gas (2DEG) in the left-hand (LH) contact. In our calculations, the injection energy and uniform electric field F in the QW are found by using a simple model for the potential variation through the device [6]. The chaos is generated by collisions with the barriers which interrupt the regular orbital motion at irregular times [6,7]. To study how the classical motion in the well evolves with θ , we have

calculated trajectories for 225 different initial directions at the LH barrier, consistent with the electron injection energy calculated from the bias voltage V across the device. Figure 2 shows Poincaré sections generated by plotting the velocity components (v_y, v_z) each time the electron hits the LH barrier when $B = 11.4$ T and $F = 2.1 \times 10^6$ V m $^{-1}$ (corresponding to 0.4 V bias voltage on the structure of Ref. [6]). At $\theta = 0^\circ$ [Fig. 2(a)], the electrons perform cyclotron motion about the magnetic field so that (v_y, v_z) lie on concentric circles. When $\theta = 3^\circ$, islands of stable orbits are surrounded by a sea of chaos. Comparison of Figs. 2(b) and 2(c) shows that the size of the chaotic sea increases with increasing θ until the system exhibits strongly chaotic behavior when $\theta = 24^\circ$ [Fig. 2(d)].

To investigate how the onset of chaotic classical motion influences the corresponding quantum mechanical energy level spectrum, we have calculated the energy levels ϵ_n for a QW of width $w = 120$ nm with impenetrable walls when $B = 11.4$ T and $F = 2.1 \times 10^6$ V m $^{-1}$. In the gauge given by the vector potential $A = (0, xB \sin\theta - zB \cos\theta, 0)$, the Hamiltonian for motion in the well,

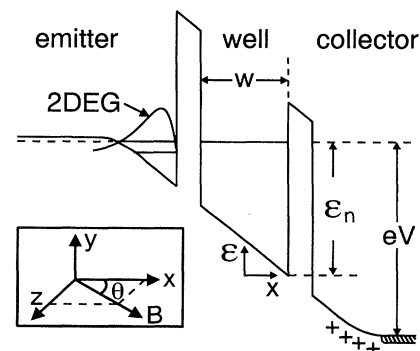


FIG. 1. Schematic conduction band diagram of the RTD under bias V showing the 2DEG in the LH contact and the energy ϵ_n of the n th level in the well. Inset: angle θ of the magnetic field relative to the tunneling (x) direction.

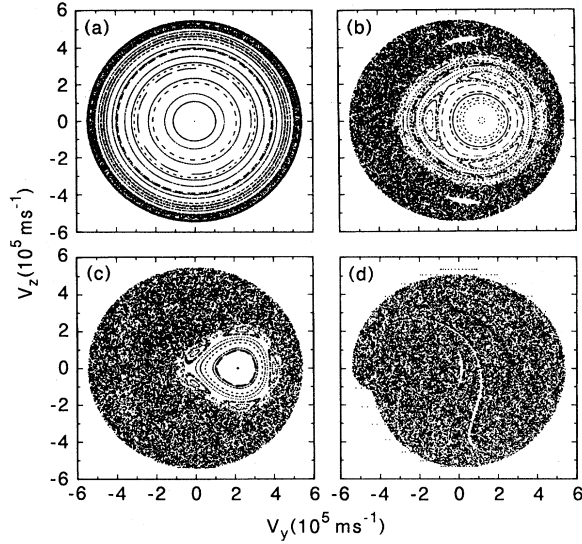


FIG. 2. Poincaré sections showing (v_y, v_z) for 22500 collisions with the LH barrier generated from 225 starting velocities with $\theta =$ (a) 0° , (b) 3° , (c) 6° , and (d) 24° .

$|x| < \frac{1}{2}w$, is

$$\hat{H} = \frac{\hat{p}_x^2 + (\hat{p}_y + exB \sin\theta - ezB \cos\theta)^2 + \hat{p}_z^2}{2m^*} + eF(\frac{1}{2}w - x),$$

where $\hat{p}_x, \hat{p}_y, \hat{p}_z$ are canonical momentum operators and $m^* = 0.067m_e$ is the band edge mass in GaAs. Because $p_y = \hbar k_y$ is a constant of the motion, we expand an eigenfunction

$$\Psi_{n,k_y}(x, y, z) = \sum_{p,l} c_{p,l}^n \sin \frac{l\pi(x + \frac{1}{2}w)}{w} \phi_p(z - z_0) \times \exp(ik_y y),$$

where $l = 1, 2, 3, \dots$ and $\phi_p(z - z_0)$ is a simple harmonic oscillator (SHO) wave function ($p = 0, 1, 2, \dots$) centered at $z_0 = \hbar k_y / eB \cos\theta$. Within this basis, the Hamiltonian reduces to a two-dimensional real symmetric matrix whose eigenvalues are the energy levels ϵ_n ($n = 1, 2, 3, \dots$) which are independent of k_y provided z_0 lies within the sample boundaries.

For energies above ~ 100 meV and for $15^\circ \leq \theta \leq 60^\circ$, the level pattern exhibits the complexity characteristic of nonintegrable systems [1,2] and will be described more fully elsewhere [8]. In this paper, we analyze the energy level spectrum for the particular tilt angle $\theta = 20^\circ$ within the domain dominated by strong classical chaos. Despite the complexity of the spectrum, periodic clustering of the energy levels occurs. This is most easily seen when each energy level is broadened to ~ 2 meV, producing the smoothed density of levels $D(\epsilon)$ shown in Fig. 3(a). In the calculations, a basis constructed from 120 sine waves and 120 SHO wave functions is used which gives accurate energy levels to at least 1.3 eV when $\theta = 20^\circ$.

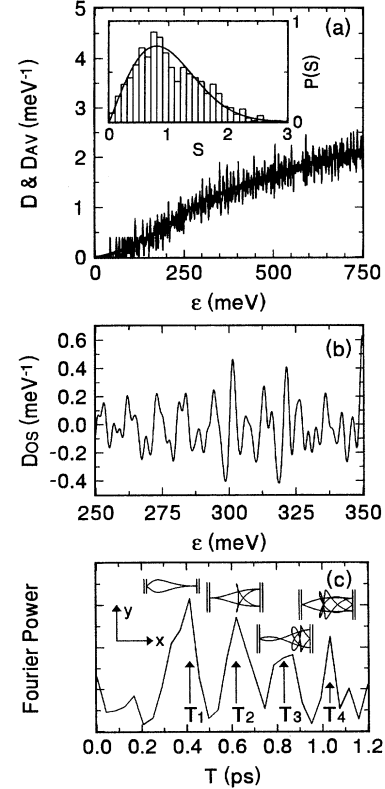


FIG. 3. (a) Slowly (rapidly) varying curve: local mean density of levels $D_{AV}(\epsilon)$ [smoothed density of levels $D(\epsilon)$] calculated for $B = 11.4$ T, $F = 2.1 \times 10^6$ V m $^{-1}$, and $\theta = 20^\circ$. Inset histogram: probability distribution $P(S)$ of scaled level spacings S for the range $100 \leq \epsilon_n \leq 700$ meV. Solid curve: $P_{GOE}(S)$. (b) Oscillatory contribution $D_{OS}(\epsilon)$ to the density of levels. (c) Fourier power spectrum of the $D_{OS}(\epsilon)$ plot showing four distinct peaks labeled by T_1, T_2, T_3, T_4 and corresponding periodic orbits shown projected on the x - y plane (axes inset).

The density of levels can be expressed as the sum of the local mean density $D_{AV}(\epsilon)$ and a rapidly oscillating term $D_{OS}(\epsilon)$ as shown in Fig. 3. In the semiclassical limit, $D_{AV}(\epsilon)$ can be calculated from phase space arguments and $D_{OS}(\epsilon)$ can be related to the unstable periodic classical orbits using the Gutzwiller trace formula [1]

$$D_{OS}(\epsilon) = \text{Im} \sum_j a_j \exp[iS_j(\epsilon, B, F, \theta)/\hbar],$$

where $S_j(\epsilon, B, F, \theta)$ is the classical action of the j th topologically distinct periodic orbit, and the expansion coefficient a_j depends on the orbital stability. For given B, F , and θ , each periodic orbit imposes a regular modulation in the density of levels with an energy period $\Delta\epsilon_j = \hbar[\partial S(\epsilon, B, F, \theta)/\partial \epsilon]^{-1} = \hbar/T_j(\epsilon, B, F, \theta)$, where $T_j(\epsilon, B, F, \theta)$ is the period of the j th unstable closed orbit. When $F = 2.1 \times 10^6$ V m $^{-1}$, electrons in the RTD are injected into the QW at energy $\epsilon_{in} \approx 300$ meV relative to the conduction band edge at the right-hand (RH) side of the well. Fig. 3(b) shows $D_{OS}(\epsilon)$ for energies close

to ϵ_{in} . Several periodic components can be identified. These are revealed more clearly in the Fourier transform shown in Fig. 3(c). The horizontal scale indicates the time $T = h/\Delta\epsilon$ corresponding to the reciprocal of the energy period. The Fourier power spectrum contains four distinct peaks with characteristic times $T_1 \sim 0.4$ ps, $T_2 \sim 0.6$ ps, $T_3 \sim 0.8$ ps, and $T_4 \sim 1.0$ ps, almost identical to the periods of the type 1, type 2, and type 3 unstable closed orbits (shown projected on the x - y plane) [6], where the type number gives the number of successive collisions on the RH barrier for each period. These are the shortest periodic orbits in the QW close to the electron injection energy. The oscillations in $D_{OS}(\epsilon)$ produced by the type 1 and type 2 orbits (two leftmost insets) have periods consistent with the series of peaks in the observed current-voltage characteristics $I(V)$ [6].

The spacings between adjacent energy levels exhibit behavior which is thought to be universal for nonintegrable systems. To investigate the statistical properties of these spacings, the energy levels $\{\epsilon_n\}$ are mapped into a new sequence of levels $\{E_n\}$ according to the transformation $E_n = N_{AV}(\epsilon_n)$ [1,2], where $N_{AV}(\epsilon)$ is the average number of levels below energy ϵ . The histogram in Fig. 3(a) shows the probability distribution of the separation S between adjacent scaled levels calculated for $\theta = 20^\circ$, $F = 2.1 \times 10^6$ V m $^{-1}$, and $B = 11.4$ T. This distribution closely resembles the Wigner probability density function $P_{GOE}(S) = (\pi S/2) \exp(-\pi S^2/4)$ shown by the solid curve [Gaussian orthogonal ensemble (GOE) statistics [1]]. This is due to the $S_y\tau$ invariance of the Hamiltonian (operator S_y changes the sign of the y coordinate and τ is the time reversal operator), which ensures that the reduced Hamiltonian matrix is real symmetric, and therefore the level spacings obey GOE statistics [9].

In the semiclassical regime, the wave functions of nonintegrable systems often reveal regions of high probability density (scars) near the paths of periodic classical orbits [1,3]. For our system, we have identified a number of unstable periodic orbits, each of which produces remarkably clear scars in individual eigenfunctions associated with subsets of regularly spaced energy levels embedded within the complete spectrum. In Fig. 4, we show probability density plots for wave functions scarred by type 1 orbits [(a) and (b)] or type 2 orbits [(c) and (d)] overlaid. In our chosen gauge, the probability density depends only on x and z [10]. For comparison, the gauge invariant classical orbits are therefore shown projected on the x - z plane. Projections on the x - y plane are also shown in the inset. The eigenfunctions reveal well-defined scars which are localized along a single closed orbit and lie approximately parallel to \mathbf{B} . The energy levels corresponding to the wave functions scarred by the type 1 (type 2) orbits in Fig. 4 are separated by $\Delta\epsilon = 9.03$ (5.55) meV, which is very close to the value $h/T = 8.99$ (5.51) meV obtained from the mean orbital period $T = 0.46$ (0.75) ps calculated at an energy midway between the two levels. Intermediate energy levels generally reveal no trace of

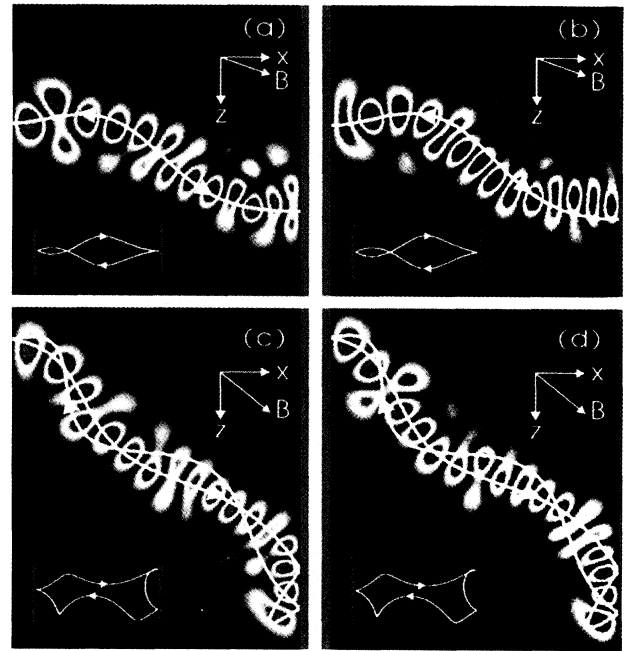


FIG. 4 (color). Probability density (black = 0) of eigenfunctions corresponding to levels: (a) $\epsilon_n = 102.83$ meV ($n = 34$) and (b) $\epsilon_n = 111.86$ meV ($n = 40$) at $\theta = 20^\circ$; (c) $\epsilon_n = 98.44$ meV ($n = 37$) and (d) $\epsilon_n = 103.99$ meV ($n = 42$) at $\theta = 40^\circ$. $F = 5.25 \times 10^5$ V m $^{-1}$ ($V = 0.1$ V), $B = 11.4$ T. Overlays: classical orbits scarring wave functions. Arrows show direction of travel. Upper insets: magnetic field orientation in x - z plane. Lower insets: orbits projected onto x - y plane (x normal to barriers).

the scars. Subsets of levels which display scarred wavefunctions can be fitted quite well by a quantization condition $S_j(\epsilon, B, F, \theta) = (\nu + \phi_j)h$, where $\nu = 1, 2, 3, \dots$ gives the number of antinodes in the scarred wave function along the closed classical path and ϕ_j is fixed for a given orbit. The scarred wave functions usually correspond to the eigenvalues closest to the energies predicted by this quantization rule.

For the successive wave functions scarred by type 1 orbits in Figs. 4(a) and 4(b), the number of antinodes is $\nu = 13$ and 14 and for this sequence $\phi_1 = 1.2$. For the scars of the type 2 orbits in Figs. 4(c) and 4(d), $\nu = 17$ and 18 with $\phi_2 = 2.58$. Quantization of the classical action thus enables us to predict which eigenfunctions will be scarred by the orbits and directly relate the quantum numbers ν to the scar patterns. This rule has successfully located scars of type 1 (type 2) orbits which are accessible to tunneling electrons in the RTD's [6] for quantum numbers in the range $17 \leq \nu \leq 29$ ($10 \leq \nu \leq 32$) and for a variety of V and θ values. Subsets of eigenstates scarred by other unstable periodic orbits can also be identified in this way. General features of scarring have been studied by Berry [11] using Wigner functions. Wigner functions for individual eigenstates were used by Agam and Fishman [12] to analyze scar patterns in a

billiard stadium. They found maximal scar strengths near energies satisfying the above quantization rule. In our system, the scar patterns clearly resemble standing waves along the classical path which has permitted a simple physical interpretation of ν . Similar results were found by Eckhardt, Hose, and Pollak [13] for the scarring of degenerate eigenstates in a chaotic quartic oscillator.

To investigate the role of eigenfunction scarring in the experimental tunneling characteristics, we must take into account the finite heights of the confining barriers in the RTD. At low energies, this perturbs only weakly the level spectra obtained for infinite barriers, but is necessary to give nonzero tunnel coupling of the QW and emitter 2DEG states. We have therefore calculated QW states for 330 meV barriers [GaAs/(Al_{0.4}Ga_{0.6})As] using a more general set of basis functions. The transfer matrix elements coupling the QW states to the occupied emitter state ($n = 0$ Landau level) were obtained for a range of energies close to the tunnel injection energy. The tunneling rate is proportional to the square of this matrix element. As shown in Fig. 5 for $V = 0.1$ V, $B = 11.4$ T, this is found to be an order of magnitude larger for the states scarred by type 2 orbits [of Figs. 4(c) and 4(d), $\theta = 40^\circ$] than for nearby unscarred states. Similar results are found for scarred states occurring at other values of V , B , and θ . This clearly demonstrates that for certain voltage regimes tunneling into individual scarred states produces periodic peaks in the tunneling rates and hence in $I(V)$, which totally dominate the weak background transitions into unscarred states. Unfortunately, experiments on the 120 nm wide well have insufficient resolution to distinguish between tunneling into a discrete scarred state or a cluster of neighboring levels since the mean level spacing ~ 1 meV is much less than the broadening $\Gamma = \hbar/\tau_s \sim 6$ meV, corresponding to the lifetime $\tau_s \sim 0.1$ ps imposed by optic phonon emission and scattering processes [14]. However, for narrower wells ~ 20 nm and higher fields $B \sim 35$ T, resonant features

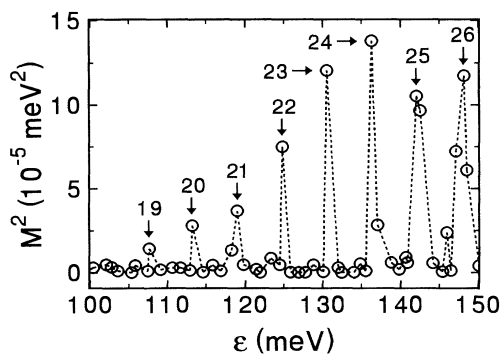


FIG. 5. Square of transfer matrix element M for tunneling into QW states at energies close to the injection energy $\epsilon_{in} = 88$ meV for $V = 0.1$ V, $B = 11.4$ T, and $\theta = 40^\circ$. Arrows indicate states scarred by type 2 periodic orbits with antinode quantum number ν shown.

in $I(V)$ originating from transitions into individual states could, in principle, be resolved. The tunnel current amplitudes could then provide direct experimental evidence for periodic wave-function scarring.

In summary, we have investigated the energy level spectrum and wave functions of a wide QW in the regime of strong classical chaos. The statistical behavior of the levels reveals clustering on a scale determined by the underlying periodic classical orbits. Sequences of individual wave functions scarred by single periodic orbits can be located using a Bohr–Sommerfeld-like quantization rule in which the quantum number is directly related to the scar pattern. Wave-function scarring has a pronounced effect on the tunneling rate into the well which exhibits pronounced maxima for transitions into individual scarred states. Magnetotunneling experiments on RTD's with narrower wells and higher magnetic fields than hitherto shown may give direct evidence for periodic wave-function scarring and resolve the question of whether the observed resonant peaks originate from transitions into *individual* scarred states or into *clusters* of levels, which both have the same energy periodicity.

EPSRC (UK) support this work and L.E. is supported by a Senior Fellowship.

-
- [1] M.C. Gutzwiller, *Chaos in Classical and Quantum Mechanics* (Springer-Verlag, New York, 1990); L.E. Reichl, *The Transition to Chaos* (Springer-Verlag, New York, 1992).
 - [2] M.V. Berry, Proc. R. Soc. London A **413**, 183 (1987).
 - [3] E.J. Heller, Phys. Rev. Lett. **53**, 1515 (1984).
 - [4] R. Fleischmann, T. Geisel, and R. Ketzmerick, Phys. Rev. Lett. **68**, 1367 (1992); D. Weiss, K. Richter, A. Menschig, R. Bergmann, H. Schweizer, K. von Klitzing, and G. Weimann, Phys. Rev. Lett. **70**, 4118 (1993).
 - [5] C.M. Marcus, A.J. Rimberg, R.M. Westervelt, P.F. Hopkins, and A.C. Gossard, Phys. Rev. Lett. **69**, 506 (1992).
 - [6] T.M. Fromhold, L. Eaves, F.W. Sheard, M.L. Leadbeater, T.J. Foster, and P.C. Main, Phys. Rev. Lett. **72**, 2608 (1994); T.M. Fromhold, M.L. Leadbeater, L. Eaves, T.J. Foster, F.W. Sheard, P.C. Main, P.J. McDonnell, and A. Fogarty, Semicond. Sci. Technol. **9**, 488 (1994).
 - [7] D.L. Shepelyansky and A.D. Stone, Phys. Rev. Lett. **74**, 2098 (1995).
 - [8] T.M. Fromhold, P.B. Wilkinson, F.W. Sheard, and L. Eaves (to be published).
 - [9] M. Robnik and M.V. Berry, J. Phys. **19**, 669 (1986).
 - [10] Although the position of the probability density plots along the z axis depends on k_y , the form of the distribution does not.
 - [11] M.V. Berry, Proc. Soc. London A **423**, 219 (1989).
 - [12] O. Agam and S. Fishman, Phys. Rev. Lett. **73**, 806 (1994).
 - [13] B. Eckhardt, G. Hose, and E. Pollak, Phys. Rev. A **39**, 3776 (1989).
 - [14] We note that for successive scarred states in Fig. 4 the energy spacing $\Delta\epsilon \approx \Gamma$.

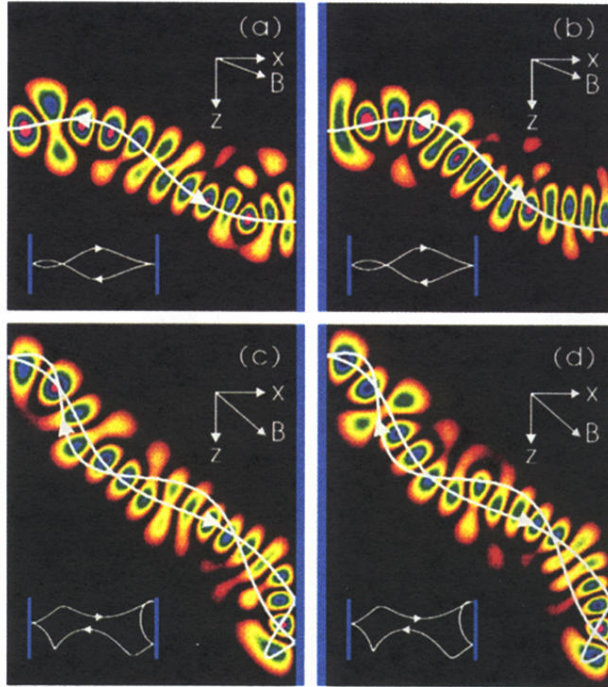


FIG. 4 (color). Probability density (black = 0) of eigenfunctions corresponding to levels: (a) $\epsilon_n = 102.83$ meV ($n = 34$) and (b) $\epsilon_n = 111.86$ meV ($n = 40$) at $\theta = 20^\circ$; (c) $\epsilon_n = 98.44$ meV ($n = 37$) and (d) $\epsilon_n = 103.99$ meV ($n = 42$) at $\theta = 40^\circ$. $F = 5.25 \times 10^5$ V m $^{-1}$ ($V = 0.1$ V), $B = 11.4$ T. Overlays: classical orbits scarring wave functions. Arrows show direction of travel. Upper insets: magnetic field orientation in x - z plane. Lower insets: orbits projected onto x - y plane (x normal to barriers).